Letter

Optical transitions near the elusive $5s$-$4f$ level crossing in highly charged osmium with sensitivity to physics beyond the standard model

Nils-Holger Rehbehn,[1] Lakshmi Priya Kozhiparambil Sajith,[1,2] Michael K. Rosner,[1] Charles Cheung,[3] Sergey G. Porsev,[3] Marianna S. Safronova,[3] Steven Worm,[2] Dmitry Budker,[4,5,6,7] Thomas Pfeifer,[1] José R. Crespo López-Urrutia,[1,*] and Hendrik Bekker[4,5,6,†]

[1]*Max-Planck-Institut für Kernphysik, D–69117 Heidelberg, Germany*

[2]*DESY, D–15738 Zeuthen, Germany*

[3]*Department of Physics and Astronomy, University of Delaware, Newark, Delaware 19716, USA*

[4]*Johannes Gutenberg-Universität Mainz, 55122 Mainz, Germany*

[5]*Helmholtz Institute Mainz, 55099 Mainz, Germany*

[6]*GSI Helmholtzzentrum für Schwerionenforschung GmbH, 64291 Darmstadt, Germany*

[7]*Department of Physics, University of California, Berkeley, California 94720-7300, USA*

(Received 22 September 2025; accepted 7 November 2025; published 5 December 2025)

Optical transitions in highly charged ions can be very sensitive to hypothetical beyond-the-standard-model phenomena. Those near the degeneracy due to the $5s$-$4f$ level crossing are especially promising. We present measurements of $Os^{15,16,17+}$ ions at an electron beam ion trap and corresponding predictions of several transitions that show a high sensitivity to hypothetical fifth forces and possible violations of local Lorentz invariance. We found electric quadrupole transitions in Os^{16+}, which are suitable for frequency metrology due to linewidths down to 44 μHz. Our calculations show the need for including enough inner-shell excitations to avoid an overestimation of interconfiguration transition rates, which were too faint for detection at the present signal-to-noise ratio.

DOI: 10.1103/p347-47ys

Introduction. Very recently, by applying quantum logic [1] to frequency metrology [2,3] of sympathetically cooled highly charged ions (HCI) [4,5], a precision close to that of state-of-the-art optical clocks [6] for neutral and singly charged atoms has been reached at the German metrology institute Physikalisch-Technische Bundesanstalt (PTB) in Braunschweig [7–13]. This enables searches for physics beyond the standard model (BSM) [14] using, e.g., King-plot analysis [15–17] to probe hypothetical Yukawa interactions, as just demonstrated at PTB [12]. The sensitivity of HCI to various BSM effects, such as variation of the fine-structure constant α, is highest near orbital crossings [18–20] where the filling order changes. However, predictions for the energy levels are extremely difficult in the interesting case of the $5s$-$4f$ orbital crossing [21–23]. Here we investigate both theoretically and experimentally one of the most promising candidates for this crossing. It was at first expected to provide laser-accessible optical transitions between fine-structure levels of the $[\mathrm{Pd}]4f^{12}5s^2$ and $[\mathrm{Pd}]4f^{13}5s$ configurations in the Nd-like iridium ($Z = 77$) Ir^{17+} ion. They were, however, not found, and recent predictions show that they should appear in the vacuum ultraviolet range instead [24,25], a region hitherto unexplored for this ion. In the present work, we study Nd-like Os^{16+} ($Z = 76$), which has a smaller splitting between the relevant configuration, with newer calculations predicting laser-accessible transitions there [26]. Moreover, the lowest excited state couples to the ground state by an ultranarrow electric quadrupole (E2) transition well suited for frequency metrology.

One advantage of HCI is the strong binding of the outer electrons [14], which are less affected by external perturbations than atoms and singly charged ions. Their wave function strongly overlaps with the nucleus, enhancing hypothetical BSM electron-neutron interactions accessible to the generalized King-plot method [27]. Osmium is very well suited for such studies, with seven stable, naturally occurring isotopes, among them five with zero nuclear spin, since its high nuclear charge causes large relativistic effects. In Os^{16+}, these are markedly different for s and f electrons, giving their interconfiguration transitions an outstanding sensitivity to a potential α variation and to hypothetical violations of local Lorentz invariance [26].

Theory. To assist line identification, we perform large-scale configuration interaction (CI) calculations for this ion, systematically accounting for correlation effects between the $[1s^2 \ldots 4d^{10}]$ closed-shell core and the 14 f valence electrons. In total, we calculate 13 low-lying even-parity energy levels and four odd-parity energy levels, see the "PCI" column of Table III. The vast number of configurations with small individual weights that arise here requires the inclusion of many to achieve convergence. We sped up by a factor of three the

*Contact author: crespojr@mpi-hd.mpg.de
†Contact author: hbekker@uni-mainz.de

TABLE I. Selection of E1 reduced matrix elements $\langle 4f^{12}5s^2\|D\|\,4f^{13}5s\rangle$ (in 10^{-3} atomic units, a.u.) and transition rates A_{ab} (in s^{-1}) in different approximations. Calculations are performed with a $7spdfg$ basis set. Predicted wavelengths λ (in nm) and their uncertainties are listed in the second column. Results obtained in the framework of 24-, 30-, and 60-electron CI are listed in columns "$4d$ open," "$4p$ open," and "all open," respectively. Final values and uncertainties listed in columns "Final" and "Uncertainty" take into account the correlation of all 60 electrons, along with other correlation corrections. Transition-rate uncertainties originate from those of D and the respective energy uncertainties.

Transition		D ($\times 10^{-3}$ a.u.)					A_{ab} (s^{-1})		
$a-b$	λ (nm)	$4d$ open	$4p$ open	all open	Final	Uncertainty	$4d$ open	Final	Uncertainty
$^3F_4$ - $^3F_4^o$	451^{+84}_{-61}	1.93	0.31	0.37	0.12	0.27	12.62	0.04	0.16
$^3H_4$ - $^3F_4^o$	555^{+135}_{-90}	2.46	2.12	1.94	1.75	0.24	4.61	4.02	2.59
$^3H_4$ - $^3F_3^o$	743^{+261}_{-153}	3.61	2.45	2.34	2.12	0.21	3.34	2.47	1.98
$^3F_4$ - $^3F_3^o$	374^{+56}_{-43}	2.43	0.91	0.99	0.87	0.17	42.95	4.19	2.35
$^3P_2$ - $^3F_2^o$	426^{+77}_{-56}	1.48	1.19	1.11	1.01	0.11	10.61	5.36	2.74
$^3P_2$ - $^1F_3^o$	543^{+132}_{-89}	2.69	1.52	1.61	1.60	0.10	16.16	6.47	3.88

Hamiltonian construction using a bitstring-determinant storage and manipulation method developed for the PCI package [28] based on Ref. [29].

We construct our basis set based on previous work with Ir^{17+} [25] expanding it to include orbitals with principal quantum number up to $n = 13$ for partial waves up to $l = 7$, and comprising all orbitals up to $13g$, $12h$, $11i$, and $10k$. We gradually expand the basis set until convergence is reached for various correlation corrections, using a reference 30-electron CI calculation (that is, allowing excitations from the $5s$, $4f$, $4d$, and $4p$ shells) with a $7spdfg$ basis set. We refer to allowing excitations from an inner shell as opening the shell.

First, we performed shell-by-shell CI calculations following Ref. [25] to account for inner-shell correlations. As in Ir^{17+}, we found the largest contributions from opening the $4d$ shell, shifting the configuration splitting by $\sim$8000 cm^{-1}, followed by opening the $4p$ and $4s$ shells, which give an overall contribution larger than the contribution from the innermost shells with $n \leqslant 3$. Although even-parity levels are largely unaffected, odd-parity levels shift by about $-2100\,cm^{-1}$. We then expand the basis set to $13g12h11i10k$ and extrapolate higher n partial-wave contributions. Allowing excitations from $4f^{14}$ leads to negligible shifts for most states. Finally, we include (i) single and double excitations from $4f^{12}5p^2$ and single excitations from six dominant odd-parity configurations within 30-electron CI, and (ii) triple excitations from $4f^{12}5s^2$ and $4f^{14}$ within 14-electron CI. The results are shown in column "PCI" of Table III, with details given in the Supplemental Material [30]. Note that for convenience we assign LS-coupled term symbols to each level based on their largest contributor even though intermediate coupling applies here due to significant relativistic effects. The largest shifts arise from including the inner shells with $n = 3, 4$, higher partial waves, and additional reference configurations. Limitations of our local computing cluster impeded the full inclusion of these effects, potentially leading to a sizable underestimation. We assign uncertainties accordingly to reflect these omissions.

We also determined electric dipole (E1), magnetic dipole (M1), and electric quadrupole (E2) transition rates by calculating respective reduced matrix elements between the investigated states. Typical selection rules for light and singly charged ions do not apply in the intermediate-coupling regime of the HCIs investigated here. Instead, the strongest optical transitions are of M1 type and they can take place between different terms due to state mixing. The E1 transitions are rather weak due to the relatively small overlap between the $5s$ and $4f$ orbitals. In our calculations we found that the E1 reduced matrix elements $\langle 4f^{12}5s^2\|D\|\,4f^{13}5s\rangle$ strongly depend on which shells are treated as open. In contrast, we find that reduced matrix elements of the M1 operator and the corresponding transition rates are only weakly affected by additional correlation corrections. For example, for the $4f^{12}5s^2\ ^3F_4$ - $4f^{13}5s\ ^3F_4^o$ E1 transition, our result at the reference $7spdfg$ level within the framework of the

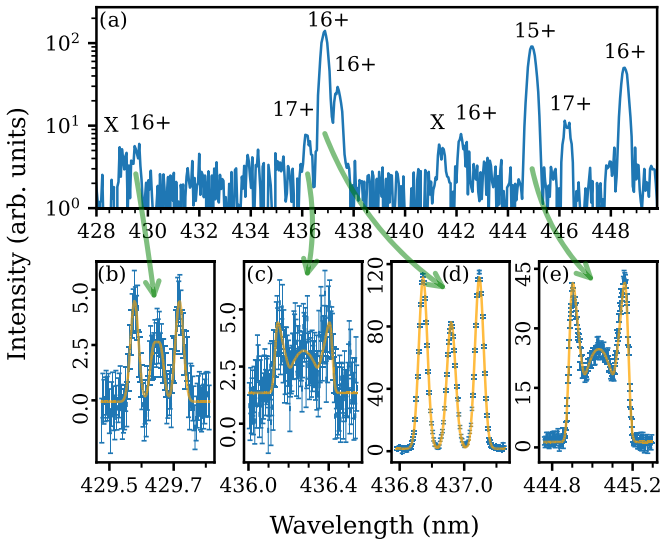

FIG. 1. Examples of spectra. (a) Overview taken with 150 grooves/mm grating showing lines of varying intensity of osmium ions in three charge states and two lines from impurities (marked with an X). Bottom: High-resolution spectra with fits of our line-shape model in orange. (b) Weakest identified transition in Os^{16+}. (c) Transition between the two lowest states of the Os^{17+} $4f^{13}$ configuration. (d) A strong Os^{16+} transition. (e) Ground state transition of Os^{15+}.

TABLE II. Measured and inferred vacuum wavelengths λ_{vac} of Os^{15+}, Os^{16+}, and Os^{17+} with identifications. Transition rates A_{ab} are based on our PCI calculations for Os^{16+} and AMBiT [39] ones for $Os^{15,17+}$. **R**: Ritz-Rydberg combination.

Config.	Transition	λ_{vac} (nm)	A_{ab} (s^{-1})	Type
Os^{15+}				
$4f^{13}5s^2$	$^2F^o_{5/2}$ - $^2F^o_{7/2}$	445.03146(63)	181	M1
Os^{16+}				
$4f^{13}5s$	$^1F_3{}^o$ - $^3F_4{}^o$	360.11375(17)	196	M1
	$^1F_3{}^o$ - $^3F_3{}^o$	429.6482(11)	6.5	M1
	$^3F_2{}^o$ - $^3F_3{}^o$	547.7247(38)	141	M1
$4f^{12}5s^2$	$^3P_1$ - $^3F_2$	242.3348(17)	91	M1
		242.34080(16) **R**		
	$^3H_4$ - $^3F_4$	247.1159(8)	13	M1
		247.11704(19) **R**		
	$^3H_4$ - $^3H_5$	356.28870(9)	249	M1
	$^3D_2$ - $^3F_2$	395.74681(36)	136	M1
	$^3F_3$ - $^3F_4$	436.95983(16)	189	M1
	$^3P_2$ - $^3D_2$	437.48246(36)	165	M1
	$^3D_2$ - $^3F_3$	448.62855(31)	129	M1
	$^3H_5$ - $^3H_6$	472.19841(26)	248	M1
	$^1G_4$ - $^3F_4$	491.79063(29)	92	M1
	$^3H_4$ - $^1G_4$	496.70195(72)	77	M1
	$^3H_4$ - $^3F_3$	568.7831(25)	8.1	M1
		568.7876(11) **R**		
	$^3P_1$ - $^3D_2$	625.17496(60)	43	M1
	$^3F_2$ - $^3F_4$	502.3391(12) **R**	3.99×10^{-3}	E2
	$^3F_4$ - $^3H_6$	1139.2103(78) **R**	4.36×10^{-5}	E2
Os^{17+}				
$4f^{13}$	$^2F^o_{5/2}$ - $^2F^o_{7/2}$	436.2751(20)	185	M1
$4f^{12}5s^1$	$^3H_{11/2}$ - $^4H_{13/2}$	363.986(21)	296	M1
$4f^{11}5s^2$	$^4I^o_{13/2}$ - $^4I^o_{15/2}$	500.689(25)	319	M1

24-electron CI (the column "4*d* open") agrees with the previous theory [26]. However, adding correlations from the 4*p* shell reduces the amplitude from 1.93×10^{-3} a.u. to 0.12×10^{-3} a.u., lowering the transition rate to below 1 s^{-1}, as shown in Table I. We attribute this effect to negative contributions from one-electron 4*p*-5*s* matrix elements. This shows that calculations neglecting inner-shell correlations are unreliable for interpreting measurements. Inclusion of the *h* partial wave further reduces the interconfiguration transition rates, likely through the cumulative effect of many small but non-negligible admixtures. Detection of such interconfiguration lines at the long sought-after 5*s*-4*f* level crossing would provide the most α-variation-sensitive transitions. Table I shows those with highest transition rates, which are therefore the most promising prospects for experimental observation. Uncertainty values for the reduced matrix elements are assigned by adding the respective contributions in quadrature. For $^3F_4$ - $^3F^o_4$, the uncertainty is greater than the value of the matrix element *D*, so *D* should be taken as an order of magnitude estimate.

Measurements. Osmium was investigated in an electron beam ion trap (EBIT) [31–33]. The Heidelberg EBIT (HD-EBIT) ran with a 40 mA, $\tilde{4}$00 eV electron beam compressed by its 8 T magnetic field. This beam radially traps approximately 3×10^6 Os^{16+} ions in its negative space-charge potential, which are moreover axially confined by biased drift tubes, forming a cylindrical cloud of 50 mm length and 0.1 mm diameter. Osmium atoms were sourced from a tenuous molecular beam of osmocene, a volatile organometallic compound that the electron beam dissociates. Sequential electron-impact ionization and suppressed charge exchange in the 4-K environment allows selection of the desired charge state by appropriately setting the electron-beam energy and axial trap depth. A rotated image of the horizontal ion cloud is focused onto the vertical entrance slit of a 2 m focal-length grating spectrometer by a set of lenses and mirrors. For calibration, a diffuse reflector illuminated by a hollow-cathode lamp is moved in and out of an intermediate image plane between lenses. A low-noise CCD camera acquires the HCI spectra with exposure times of 1 h. Dark images without

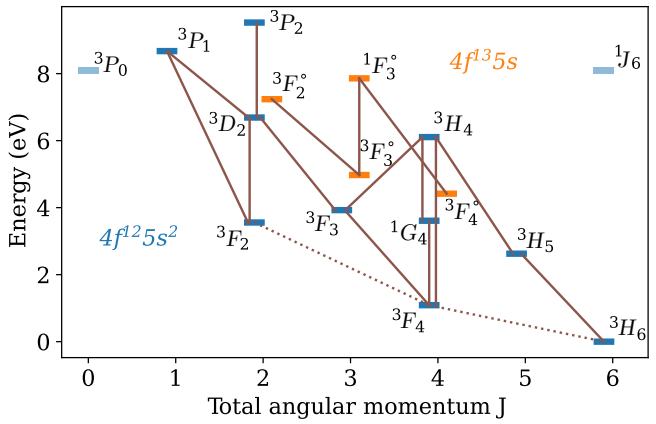

FIG. 2. Level scheme of Os^{16+} based on the present measurements, cf. Table III. M1 transitions shown as solid lines; E2 clock transitions are dashed. Disconnected levels and the interconfiguration splitting taken from our PCI predictions.

trapped ions are recorded to remove the stray light background and correct for the sensitivity of each camera pixel. Calibrations at regular intervals remove the effect of thermal and mechanical drifts of the spectrometer. These procedures allowed us to reach wavelength fractional uncertainties as low as $\Delta\lambda/\lambda = 2.5 \times 10^{-7}$ [16,17,22,34–38].

Our initial observations with a broadband 150 grooves/mm grating blazed for 500 nm to cover the region 316–810 nm and a 1800 grooves/mm holographic grating for the 227–323 nm range showed many $Os^{15,16,17+}$ lines, including very weak ones. Here, a broad entrance slit width of 150 µm yielded strong signal at low resolution. We set three different electron-beam energies for determining the emitting charge states based on the line intensities. Next, lines assigned to Os^{16+} and some belonging to Os^{15+} and Os^{17+} were remeasured at high resolving power using gratings with 1800 grooves/mm or 3600 grooves/mm grating and a 60 µm slit. In some cases, we measured the lines in second diffraction order for higher resolution and access to more calibration lines. Each HCI line was recorded for at least 7 h, while up to 34 h were spent on weak ones.

Identifications. We assigned lines to Os^{16+} by comparison of their predicted wavelengths and characteristic Zeeman splitting in the 8 T field of HD-EBIT. We modeled the line shape based on the total angular moment J and the predicted g_J factors (see Table III). The hyperfine structure of the ^{187,189}Os isotopes was not resolvable. Relative amplitudes of the Zeeman components were derived from Clebsch-Gordan coefficients of the $|J, m_J\rangle$ states and accounting for the multipole-radiation patterns. Fitting this model gave us unambiguous identification of 15 M1 transitions within configurations (see Fig. 1 and Table II). Several identifications are also supported by previous analysis of wavelength scaling laws versus nuclear charge [22]. We measured the transitions connecting the $^3P_1$-$^3F_2$ states and $^3H_4$-$^3F_3$ and also by analyzing those going through an intermediate state, as shown in Fig. 2; such Ritz-Rydberg combinations also confirm our identifications.

Our M1 line identifications fully reconstruct the fine structure of the Os^{16+} $4f^{13}5s$ configuration and nearly the full $4f^{12}5s^2$ one, with levels listed in Table III and displayed in Fig. 2. Our most advanced PCI calculations agree best out of all theory predictions with an average deviation of only 0.6% from experimental values. Based on the experimental level energies, we locate the ultranarrow E2 transitions from the $^3H_6$ ground state to the first excited state $^3F_4$ with an uncertainty

TABLE III. Level energies of Os^{16+} based on measured transitions (see Table II) with fitted g factors, compared with calculations from Ref. [26] and from this work using AMBIT [39], FAC [40], and PCI.

		Measured		Ref. [26]		AMBIT		FAC	PCI	
Config.	Level	E (eV)	g-factor	E (eV)	g-factor	E (eV)	g-factor	E (eV)	E (eV)	g-factor
$4f^{12}5s^2$	$^3H_6$	0	1.147(2)	0	1.164	0	1.164	0	0	1.164
	$^3F_4$	1.0883346(74)	1.137(5)	1.188	1.137	1.133	1.138	1.235	1.101(10)	1.142
	$^3H_5$	2.6256801(14)	1.017(3)	2.781	1.033	2.672	1.033	2.618	2.611(16)	1.033
	$^3F_2$	3.556472(13)	0.99(6)	3.803	0.824	3.724	0.834	3.950	3.585(61)	0.837
	$^1G_4$	3.6094115(59)	0.986(5)	3.799	0.989	3.690	0.992	3.688	3.602(17)	0.989
	$^3F_3$	3.9257624(84)	1.060(5)	4.157	1.083	4.057	1.083	4.128	3.928(36)	1.083
	$^3H_4$	6.1055603(23)	0.904(5)	6.210	0.927	6.215	0.920	6.155	6.085(37)	0.920
	$^3D_2$	6.689389(10)	1.119(4)	7.196	1.130	6.998	1.124	7.311	6.734(119)	1.129
	$^1J_6$	–	–	–	–	8.325	1.0026	8.579	8.091(169)	1.003
	$^3P_0$	–	–	–	–	8.449	0	8.980	8.088(186)	0
	$^3P_1$	8.672581(12)	1.469(12)	–	–	9.117	1.500	9.565	8.745(192)	1.500
	$^3P_2$	9.523428(13)	1.188(4)	–	–	9.916	1.209	10.257	9.565(138)	1.201
$4f^{13}5s$	$^3F_4^o$	x	1.254(4)	4.080	1.250	3.702	1.250	3.416	3.853(433)	1.250
	$^3F_3^o$	x+0.5572030(88)	1.042(4)	4.641	1.0524	4.297	1.054	4.006	4.416(433)	1.053
	$^3F_2^o$	x+2.820826(24)	0.663(4)	–	–	6.562	0.667	6.147	6.652(423)	0.667
	$^1F_3^o$	x+3.4429177(15)	1.043(5)	–	–	7.226	1.029	6.830	7.283(425)	1.030
$4f^{14}$	$^1S_0$	–	0	–	–	14.155	0	14.491	12.786	0

of 9.3 GHz and from there to the $^3F_2$ state with 0.584 GHz uncertainty (see Table II). This narrows the search range for precision laser spectroscopy with methods recently developed at PTB [10,11]. Subsequent quantum logic spectroscopy on these E2 transitions using auxiliary M1 lines could result in an optical atomic clock of exceptional accuracy and highest sensitivity to local Lorentz invariance [9,26].

Having identified all strong lines as M1 transitions, the remaining weak ones could be due to the strongest E1 interconfiguration transitions, such as the ones listed in Table I. Beyond transition rates, observed line intensities also depend on the mechanisms populating their upper states and the detection efficiency of the setup. We identified the $^3H_4$-$^3F_3$ transition, having a predicted rate of 6.5 s^{-1} with a signal-to-noise ratio (SNR) of 5. Therefore, the E1 transition from the same upper level $^3H_4$ to $^3F_4^o$ was expected to have an SNR only slightly above 1, and the one to $^3F_3^o$ should be too undetectable due to a grating efficiency far from its optimum. We find several unidentified candidates for the former transition in the recorded spectra, but either their line shapes did not match the predicted one, or were too weak to measure accurately. They could also be M1 transitions between higher metastable states [38], or originate from Ba or W impurity ions (from the cathode material) present in the trap and not eliminated by our adjustments of trapping potential and regular reloading of osmium sample.

To predict intensities of other E1 lines we rely on level populations predicted using the collisional radiative modeling (CRM) module of the flexible atomic code [40]. Our previous work on line intensities in the extreme ultraviolet spectrum of Os^{16+} showed that the relative steady-state populations can differ by orders of magnitude [41] from each other. We confirm the accuracy of the current predictions in the optical range by comparing the intensity of two simultaneously measured, closely spaced lines at 437 nm, where differences in detection efficiency are negligible. CRM calculations yield a population ratio in the upper states $P(^3F_3)/P(^3P_2) = 6.5$, which, together with the predictions from Table II, leads to a predicted intensity ratio of 5.7, close to the measured value of 5.3. Combining these results with the predicted E1 rates and detector efficiency shows that the sought-after interconfiguration lines are too weak to be definitively detected at the present SNR.

Several strong M1 lines of Os^{15+} and Os^{17+} were also identified (see Table II). For those, level energies with an accuracy of approximately 2%, g_J factors and transition rates were also calculated using ambit [39]. Although not all transitions were measured at high resolving power, the uncertainties are sufficiently small to enable laser searches in a reasonable time [11]. The transitions found here are suitable for generalized King-plot searches of a hypothetical fifth force using several transitions in different isotopes [12,27].

Conclusions. We measured a large set of forbidden optical M1 transitions in $Os^{15+,16+,17+}$ ions and experimentally determined most level energies of the Os^{16+} $4f^{12}5s^2$ and $4f^{13}5s$ level-crossing configurations. These are in excellent agreement with our theory, which furthermore predicts the interconfiguration E1 transition rates to be much lower than previously predicted, due to insufficient consideration of inner-shell excitations. While interconfiguration transitions remained undetectable, the high sensitivity of our experimental setup provided accurate wavelengths determination of spontaneously emitting weak M1 optical transitions. Longer exposure times and background reduction could allow detection of the even weaker interconfiguration transitions if branching ratios are favorable. We also discovered two ultranarrow clock transitions in Os^{16+} that are suitable for frequency metrology and searches for local Lorentz invariance. Frequency metrology of the reported ground-state transitions in the seven stable osmium isotopes is expected to yield excellent sensitivity to a hypothetical fifth force using the generalized King-plot method [12,27].

Acknowledgments. H.B. and J.R.C.L.-U. thank Julian Berengut for helpful discussions. The project was supported by the Max-Planck Society, the Max-Planck–Riken–PTB–Center for Time, Constants and Fundamental Symmetries and the Helmholtz Association of German research Centres. The theoretical work has been supported in part by the US NSF Grant No. PHY-2309254, US Office of Naval Research Grant No. N000142512105, and by the European Research Council (ERC) under the Horizon 2020 Research and Innovation Program of the European Union (Grant Agreement No. 856415). This work has received funding from the European Partnership on Metrology, cofinanced by the European Union's Horizon Europe Research and Innovation Programme and by the Participating States, under Grant No. 23FUN03 HIOC. The calculations in this work were done through the use of Information Technologies resources at the University of Delaware, specifically the high-performance Caviness and DARWIN computer clusters. H.B. was supported in part by the project "Quantum Sensing for Fundamental Physics (QS4Physics)" funded by the Innovation pool of the research field Helmholtz Matter of the Helmholtz Association. This work is supported with funds from the Ministry of Science, Research and Culture of the State of Brandenburg within the Center for Quantum Technology and Applications (CQTA).

Data availability. The data that support the findings of this Letter are not publicly available upon publication because it is not technically feasible and/or the cost of preparing, depositing, and hosting the data would be prohibitive within the terms of this research project. The data are available from the authors upon reasonable request.

[1] P. O. Schmidt, T. Rosenband, C. Langer, W. M. Itano, J. C. Bergquist, and D. J. Wineland, Spectroscopy using quantum logic, Science **309**, 749 (2005).

[2] S. A. Diddams, D. J. Jones, J. Ye, S. T. Cundiff, J. L. Hall, J. K. Ranka, R. S. Windeler, R. Holzwarth, T. Udem, and T. W. Hänsch, Direct link between microwave and optical frequencies with a 300 THz femtosecond laser comb, Phys. Rev. Lett. **84**, 5102 (2000).

[3] R. Holzwarth, T. Udem, T. W. Hänsch, J. C. Knight, W. J. Wadsworth, and P. S. J. Russell, Optical frequency synthe-

sizer for precision spectroscopy, Phys. Rev. Lett. **85**, 2264 (2000).
[4] L. Schmöger, O. O. Versolato, M. Schwarz, M. Kohnen, A. Windberger, B. Piest, S. Feuchtenbeiner, J. Pedregosa-Gutierrez, T. Leopold, P. Micke, A. K. Hansen, T. M. Baumann, M. Drewsen, J. Ullrich, P. O. Schmidt, and J. R. C. López-Urrutia, Coulomb crystallization of highly charged ions, Science **347**, 1233 (2015).
[5] S. Chen, Z. Zhou, G. Zhang, J. Xiao, Y. Huang, and H. Guan, Coulomb crystallization of highly charged Ni^{12+} ions in a linear paul trap, Phys. Rev. A (2025).
[6] A. D. Ludlow, M. M. Boyd, J. Ye, E. Peik, and P. O. Schmidt, Optical atomic clocks, Rev. Mod. Phys. **87**, 637 (2015).
[7] P. Micke, T. Leopold, S. A. King, E. Benkler, L. J. Spieß, L. Schmöger, M. Schwarz, J. R. Crespo López-Urrutia, and P. O. Schmidt, Coherent laser spectroscopy of highly charged ions using quantum logic, Nature (London) **578**, 60 (2020).
[8] S. A. King, L. J. Spieß, P. Micke, A. Wilzewski, T. Leopold, J. R. Crespo López-Urrutia, and P. O. Schmidt, Algorithmic ground-state cooling of weakly coupled oscillators using quantum logic, Phys. Rev. X **11**, 041049 (2021).
[9] S. A. King, L. J. Spieß, P. Micke, A. Wilzewski, T. Leopold, E. Benkler, R. Lange, N. Huntemann, A. Surzhykov, V. A. Yerokhin, J. R. Crespo López-Urrutia, and P. O. Schmidt, An optical atomic clock based on a highly charged ion, Nature (London) **611**, 43 (2022).
[10] C. Cheung, S. G. Porsev, D. Filin, M. S. Safronova, M. Wehrheim, L. J. Spieß, S. Chen, A. Wilzewski, J. R. Crespo López-Urrutia, and P. O. Schmidt, Finding the ultranarrow $^3P_2 \rightarrow {}^3P_0$ electric quadrupole transition in Ni^{12+} ion for an optical clock, Phys. Rev. Lett. **135**, 093002 (2025).
[11] S. Chen, L. J. Spieß, A. Wilzewski, M. Wehrheim, K. Dietze, I. Vybornyi, K. Hammerer, J. R. Crespo López-Urrutia, and P. O. Schmidt, Identification of highly forbidden optical transitions in highly charged ions, Phys. Rev. Appl. **22**, 054059 (2024).
[12] A. Wilzewski, L. J. Spieß, M. Wehrheim, S. Chen, S. A. King, P. Micke, M. Filzinger, M. R. Steinel, N. Huntemann, L. I. Huber, J. Flannery, R. Matt, M. Stadler, R. Oswald, F. Schmid, D. Kienzler, J. Home, D. P. L. A. Craik *et al.*, Nonlinear calcium King plot constrains new bosons and nuclear properties, Phys. Rev. Lett. **134**, 233002 (2025).
[13] L. J. Spieß, S. Chen, A. Wilzewski, M. Wehrheim, J. Gilles, A. Surzhykov, E. Benkler, M. Filzinger, M. Steinel, N. Huntemann, C. Cheung, S. G. Porsev, A. I. Bondarev, M. S. Safronova, J. R. Crespo López-Urrutia, and P. O. Schmidt, Excited-state magnetic properties of carbon-like Ca^{14+}, Phys. Rev. Lett. **135**, 043002 (2025).
[14] M. G. Kozlov, M. S. Safronova, J. R. Crespo López-Urrutia, and P. O. Schmidt, Highly charged ions: Optical clocks and applications in fundamental physics, Rev. Mod. Phys. **90**, 045005 (2018).
[15] J. C. Berengut, D. Budker, C. Delaunay, V. V. Flambaum, C. Frugiuele, E. Fuchs, C. Grojean, R. Harnik, R. Ozeri, G. Perez, and Y. Soreq, Probing new long-range interactions by isotope shift spectroscopy, Phys. Rev. Lett. **120**, 091801 (2018).
[16] N.-H. Rehbehn, M. K. Rosner, H. Bekker, J. C. Berengut, P. O. Schmidt, S. A. King, P. Micke, M. F. Gu, R. Müller, A. Surzhykov, and J. R. Crespo López-Urrutia, Sensitivity to new physics of isotope-shift studies using the coronal lines of highly charged calcium ions, Phys. Rev. A **103**, L040801 (2021).
[17] N.-H. Rehbehn, M. K. Rosner, J. C. Berengut, P. O. Schmidt, T. Pfeifer, M. F. Gu, and J. R. Crespo López-Urrutia, Narrow and ultranarrow transitions in highly charged Xe ions as probes of fifth forces, Phys. Rev. Lett. **131**, 161803 (2023).
[18] J. C. Berengut, V. A. Dzuba, and V. V. Flambaum, Enhanced laboratory sensitivity to variation of the fine-structure constant using highly charged ions, Phys. Rev. Lett. **105**, 120801 (2010).
[19] J. C. Berengut, V. A. Dzuba, V. V. Flambaum, and A. Ong, Electron-Hole transitions in multiply charged ions for precision laser spectroscopy and searching for variations in α, Phys. Rev. Lett. **106**, 210802 (2011).
[20] J. C. Berengut, V. A. Dzuba, V. V. Flambaum, and A. Ong, Highly charged ions with $E1$, $M1$, and $E2$ transitions within laser range, Phys. Rev. A **86**, 022517 (2012).
[21] D. K. Nandy and B. K. Sahoo, Highly charged W^{13+}, Ir^{16+}, and Pt^{17+} ions as promising optical clock candidates for probing variations of the fine-structure constant, Phys. Rev. A **94**, 032504 (2016).
[22] A. Windberger, J. R. Crespo López-Urrutia, H. Bekker, N. S. Oreshkina, J. C. Berengut, V. Bock, A. Borschevsky, V. A. Dzuba, E. Eliav, Z. Harman, U. Kaldor, S. Kaul, U. I. Safronova, V. V. Flambaum, C. H. Keitel, P. O. Schmidt, J. Ullrich, and O. O. Versolato, Identification of the predicted $5s$-$4f$ level crossing optical lines with applications to metrology and searches for the variation of fundamental constants, Phys. Rev. Lett. **114**, 150801 (2015).
[23] U. I. Safronova, V. V. Flambaum, and M. S. Safronova, Transitions between the $4f$-core-excited states in Ir^{16+}, Ir^{17+}, and Ir^{18+} ions for clock applications, Phys. Rev. A **92**, 022501 (2015),.
[24] H. X. Liu, Y. M. Yu, B. B. Suo, Y. F. Ge, and Y. Liu, Relativistic configuration-interaction and coupled-cluster calculations of Ir^{17+} transition energies and properties for optical clock applications, Phys. Rev. A **111**, 053107 (2025).
[25] C. Cheung, M. S. Safronova, S. G. Porsev, M. G. Kozlov, I. I. Tupitsyn, and A. I. Bondarev, Accurate prediction of clock transitions in a highly charged ion with complex electronic structure, Phys. Rev. Lett. **124**, 163001 (2020).
[26] V. A. Dzuba and V. V. Flambaum, Os^{16+} and Ir^{17+} ions as candidates for accurate optical clocks sensitive to physics beyond the standard model, Phys. Rev. A **108**, 053111 (2023).
[27] J. C. Berengut, C. Delaunay, A. Geddes, and Y. Soreq, Generalized King linearity and new physics searches with isotope shifts, Phys. Rev. Res. **2**, 043444 (2020).
[28] C. Cheung, M. G. Kozlov, S. G. Porsev, M. S. Safronova, I. I. Tupitsyn, and A. I. Bondarev, pCI: A parallel configuration interaction software package for high-precision atomic structure calculations, Comput. Phys. Commun. **308**, 109463 (2025).
[29] P. Knowles and N. Handy, A new determinant-based full configuration interaction method, Chem. Phys. Lett. **111**, 315 (1984).
[30] See Supplemental Material at http://link.aps.org/supplemental/10.1103/p347-47ys for details of computations for Os^{16+}.
[31] M. A. Levine, R. E. Marrs, J. R. Henderson, D. A. Knapp, and M. B. Schneider, The electron beam ion trap: A new instrument for atomic physics measurements, Phys. Scr. **T22**, 157 (1988).
[32] M. A. Levine, R. E. Marrs, J. N. Bardsley, P. Beiersdorfer, C. L. Bennett, M. H. Chen, T. Cowan, D. Dietrich, J. R. Henderson, D. A. Knapp, A. Osterheld, B. M. Penetrante, M. B. Schneider, and J. H. Scofield, The use of an electron beam ion trap in the

study of highly charged ions, Nucl. Instrum. Meth. Phys. Res. B **43**, 431 (1989).

[33] J. R. Crespo López-Urrutia, A. Dorn, R. Moshammer, and J. Ullrich, The Freiburg electron beam ion trap/source project FreEBIT, Phys. Scr. **T80**, 502 (1999).

[34] I. Draganić, J. R. Crespo López-Urrutia, R. DuBois, S. Fritzsche, V. M. Shabaev, R. S. Orts, I. I. Tupitsyn, Y. Zou, and J. Ullrich, High precision wavelength measurements of QED-sensitive forbidden transitions in highly charged argon ions, Phys. Rev. Lett. **91**, 183001 (2003).

[35] R. S. Orts, Z. Harman, J. R. Crespo López-Urrutia, A. N. Artemyev, H. Bruhns, A. J. G. Martínez, U. D. Jentschura, C. H. Keitel, A. Lapierre, V. Mironov, V. M. Shabaev, H. Tawara, I. I. Tupitsyn, J. Ullrich, and A. V. Volotka, Exploring relativistic many-body recoil effects in highly charged ions, Phys. Rev. Lett. **97**, 103002 (2006).

[36] H. Bekker, C. Hensel, A. Daniel, A. Windberger, T. Pfeifer, and J. R. Crespo López-Urrutia, Laboratory precision measurements of optical emissions from coronal iron, Phys. Rev. A **98**, 062514 (2018).

[37] H. Bekker, A. Borschevsky, Z. Harman, C. H. Keitel, T. Pfeifer, P. O. Schmidt, J. R. Crespo López-Urrutia, and J. C. Berengut, Detection of the $5p$–$4f$ orbital crossing and its optical clock transition in Pr^{9+}, Nature Commun. **10**, 5651 (2019).

[38] M. K. Rosner, N.-H. Rehbehn, and J. R. Crespo López-Urrutia, Experimental and theoretical Ritz–Rydberg analysis of the electronic structure of highly charged ions of lead and bismuth by optical spectroscopy, J. Phys. B **57**, 055001 (2024).

[39] E. Kahl and J. Berengut, AMBiT: A programme for high-precision relativistic atomic structure calculations, Comput. Phys. Commun. **238**, 232 (2019).

[40] M. F. Gu, The flexible atomic code, Can. J. Phys. **86**, 675 (2008).

[41] H. Bekker, O. O. Versolato, A. Windberger, N. S. Oreshkina, R. Schupp, T. M. Baumann, Z. Harman, C. H. Keitel, P. O. Schmidt, J. Ullrich, and J. R. Crespo López-Urrutia, Identifications of $5s_{1/2} - 5p_{3/2}$ and $5s^2 - 5s5p$ EUV transitions of promethium-like Pt, Ir, Os, and Re, J. Phys. B: At. Mol. Opt. Phys. **48**, 144018 (2015).